PAPER

Check for updates

Eco-friendly integration of gold nanoparticles into additive manufacturing filaments: advancing conductivity and electrochemical performance†

Elena Bernalte, [iD] ‡[a] Karen K. L. Augusto, [iD] ‡[ab] Robert D. Crapnell, [iD][a] Hayley G. Andrews,[a] Orlando Fatibello-Filho [iD][b] and Craig E. Banks [iD] *[a]

This work reports the inclusion of gold nanoparticles within conductive additive manufacturing filament for an improved electrochemical and electroanalytical performance. An eco-friendly synthesis was utilised, where graphite flakes are used as a natural reducing agent for the formation of gold nanoparticles. In this way, the graphite acts as both a reducing agent and contributes to the conductivity of the filament. The presence of gold nanoparticles on the surface of the graphite was confirmed through SEM, EDX, XRD and XPS analysis, after which the graphite was thermally mixed into recycled PLA along with carbon black and castor oil to create the conductive filament. Electrodes printed from this filament produced an enhanced electrochemical performance with a ΔE_p of 111 (±5) mV, a heterogeneous electron (charge) transfer rate constant, using hexaammineruthenium(III) chloride, of k^0 of 2.04 (±0.08) × 10^{-3} cm s^{-1}, and the real electrochemical surface area, A_{real} of 0.53 (± 0.04) cm^2 upon the inclusion of gold nanoparticles. This filament also provided a significantly enhanced electroanalytical performance toward the proof-of-concept determination of lead(II), producing a linear range between 1–75 ppb (µg L^{-1}), with a sensitivity of 37 nA ppb^{-1}, an R^2 value of 0.98 and a limit of detection and limit of quantification of 0.89 ppb and 2.97 ppb, respectively. The electrodes were additionally successfully applied toward the determination of lead(II) within river water samples. This work demonstrates how advancements in the production of conductive additive manufacturing filaments can be achieved, paving the way for new research opportunities while adhering to eco-friendly practices.

1. Introduction

Additive manufacturing electrochemistry is a rapidly expanding field, stemming primarily from the synergy between the two techniques. Additive manufacturing, commonly referred to as 3D-printing, operates through the production of objects in a layer-by-layer fashion. Among the multiple types of additive manufacturing methods, the most popular in the field of electrochemistry is fused filament fabrication (FFF), also known as fused deposition modelling (FDM). This process involves depositing layers of thermoplastic polymer and offers several significant advantages over traditional formative and subtractive manufacturing techniques. These benefits include low

equipment and material costs, on-demand production, minimal to near-zero waste, cost-effectiveness for small production runs, high customizability and the ability to create complex geometries.[1,2] This method has gained significant attention within the field of electrochemistry due to its compatibility with commercially available conductive filament, leading to its application in producing lab equipment,[3] accessories,[4] and electrodes[5] in particular for electroanalytical sensors.[6–9] Although interesting, this commercially available filament has poor conductivity and even with optimisation of printing,[10–13] activation of materials[14–17] or advanced designs, the electrodes produced are nowhere close to performing like classical electrodes. To fully harness the potential of additive manufacturing in electrochemistry, researchers have shifted their focus toward developing their own unique filament formulations which through various studies have now been shown to offer exceptional electrochemical performance,[18] marking a significant advancement in the field.

Within the literature, the vast majority of custom conductive filaments reported are made using poly(lactic acid) (PLA) as the base polymer, mimicking the commercially available alternative. Among them, bespoke conductive filaments produced through thermal mixing technology is

[a] *Faculty of Science and Engineering, Manchester Metropolitan University, Dalton Building, Chester Street, M1 5GD, Great Britain, UK. E-mail: c.banks@mmu.ac.uk; Tel: +44 (0)1612 471196*

[b] *Laboratório de Analítica, Bioanalítica, Biosensores, Electroanalítica e Sensores, Departamento de Química, Universidade Federal de São Carlos (UFSCar), CP 676, 13560-970 São Carlos-SP, Brazil*

† Electronic supplementary information (ESI) available. See DOI: https://doi.org/10.1039/d4lf00368c

‡ Indicates joint first authorship.

© 2025 The Author(s). Published by the Royal Society of Chemistry

RSC Appl. Interfaces, 2025, **2**, 439–450 | **439**

preferred due to the removal of hazardous solvents from the fabrication process,[18] however when using PLA these formulations require the utilisation of an additional plasticiser compound. This ensures adequate low-temperature flexibility of the filament for 3D printing, whilst allowing high enough loadings of conductive fillers to achieve the electrochemical performance desired. Some examples have shown the use of different plasticisers such as poly(ethylene glycol),[19] poly(ethylene succinate),[20] tris(2-ethylhexyl) trimellitate,[21] and bio-based castor oil.[22]

Initially, simple utilisation of a plasticiser with loadings of 25 wt% carbon black within PLA allowed to produce filament that had resistance values ~5 times lower than the commercially available filament.[20,21] Researchers have since built on this approach by using mixed carbon materials, synergising their unique electrical, economical, and structural properties leading to significant enhancement in the filaments' performance. For example, the combination of carbon black (CB) and graphite greatly reduced the material cost of the filament without compromising the electrochemical performance,[23] while the addition of multi-walled carbon nanotubes (MWCNTs) alongside CB resulted in a filament with significantly enhanced electrochemical properties.[24] A more recent study has reported the successful integration of high loadings (up to 35 wt%) of conductive carbons within PLA filament,[25] enabling additively manufactured electrodes to perform comparably to commercially purchased electrodes in regards to their electrochemical and electroanalytical performance. So far within the literature, most bespoke conductive filaments produced have relied solely on carbon allotropes. However, Koukouviti et al.[26] reported recently a notable advancement by incorporating bismuth and copper nanopowders within filament for use in electroanalytical sensors, marking an important step forward in the field. For additive manufacturing electrochemistry to continue advancing, the development of filaments with alternative high-performance materials is required.

Gold nanoparticles (AuNPs) are one of the most seen electrode modifiers within electrochemistry. They have attractive electronic, optical, thermal, and catalytic properties, which has seen them garner attention across the scientific disciplines. Specifically for electroanalytical sensing and biosensing applications, AuNPs are especially interesting due to their biocompatibility, excellent conductivity and high surface-to-volume ratio[27] as well as their particular ability to form thiol bonds with organic molecules, enabling AuNPs to feature in devices with high sensitivity.[28] These properties have led to their inclusion within a plethora of sensing platforms for small molecules,[29] heavy metals,[30] and biosensors.[31] The use of gold has been explored within additive manufacturing, but only through post print modification such as sputtering,[32] chemical formation overnight,[33] and gold plating.[34] These steps, although improving electrode performance, add in costly and lengthy steps post-print, which negate many of the advantages that additive manufacturing brings. As such, the development of filament for FFF that already contains embedded AuNPs within

the polymer matrix would not only represent a significant breakthrough but would pave the way for a more efficient and scalable production of AuNP-based sensors and biosensors. This would contribute making additive manufacturing a viable platform for high performance electroanalytical approaches and offer a more realistic route to commercialisation.

The synthesis of AuNPs has been reported in numerous ways such as the Turkevich citrate reduction method,[35] Enustun and Turkevich method[36] and modifications of this,[37] although incorporation of solution formed nanoparticles into thermoplastics suitable for additive manufacturing could prove difficult. We therefore look to methodologies for the formation of AuNPs directly onto the carbon particles, which could then be incorporated into the filament. Strategies for the reduction of AuNPs on carbon allotropes has been reported for graphene,[38] MWCNTs,[39] and for graphite.[40] Graphite is an intriguing option as it is a naturally occurring allotrope of carbon and can therefore improve the sustainability of filaments,[23,25] building upon the use of recycled polymers[20,41,42] and bio-based plasticisers.[22] This is important for this area to conform to the UN's Sustainable Development Goals, in particular "Goal 12 – Sustainable Consumption and Production".[43] Of the reports of AuNP synthesis on graphite, many are not very environmentally friendly due to the use of large amounts of chemicals and/or complicated procedures and equipment.[44,45] However, Pandey et al.[45] report an eco-friendly synthesis of metallic nanoparticles on a piece of untreated graphite, by simply immersing into the metal salt solution where the nanoparticles are formed without the use of any reducing agent. Due to the amount of active surface defects within graphite, many functional group modifications are present, such as hydroxyl groups. These groups effectively act as reducing agents for the metal ions in solution to form metallic nanoparticles directly on the surface of the graphite.

Therefore, in this work we propose for the first time the synthesis of AuNPs onto graphite flakes utilising the facile eco-friendly synthesis, followed by the incorporation into additive manufacturing feedstock from recycled PLA. We aim to prepare the first high-performance conductive filament with embedded AuNPs that does not require specific printing conditions and post-production modifications. This material has the potential to expand the scope of additive manufacturing electrochemistry across various fields and increase the commercialisation prospects. Additionally, it aligns with the UNs Sustainable Development Goals by applying a green and energy-efficient synthesis method, incorporating biobased plasticisers, and using recycled PLA as the base polymer.

2. Experimental section

2.1 Chemicals

All chemicals used throughout this work were used as received without any further purification. All aqueous solutions were prepared with deionised water of a measured resistivity not less than 18.2 MΩ cm, sourced from a Milli-Q Integral 3 system

from Millipore UK (Watford, UK). Hexaammineruthenium(III) chloride (98%), castor oil, potassium ferricyanide (99%), potassium ferrocyanide (98.5–102%), sodium hydroxide (>98%), potassium chloride (99.0–100.5%), gold(III) chloride trihydrate (≥99.9%), lead standard for AAS (1000 ± 4 mg L^{-1}), graphite powder (<20 μm), nitric acid (70%) and hydrochloric acid (37%) were purchased from Merck (Gillingham, UK). Carbon black was purchased from PI-KEM (Tamworth, UK). Recycled poly(lactic acid) (rPLA) was purchased from Gianeco (Turin, Italy). River water samples were obtained in accordance with EPA guidelines from the River Irwell, Greater Manchester, UK (approx. location: 53.517464, −2.302739).

2.2 Synthesis of gold nanoparticles (AuNPs) on graphite

The AuNPs were synthesised onto graphite flakes adapting the method reported by Pandey et al.[45] Briefly, a 50 mL solution of gold(III) chloride trihydrate (20 mg mL^{-1}) was prepared, to which 20 g of graphite powder was added. This was placed on a stirrer plate at room temperature and left to stir overnight, after which the solution was removed through vacuum filtration using a paper filter and dried at 60 °C for at least 4 h. This powder was then ready for use within filament production.

2.3 Recycled filament production

All recycled polylactic acid (rPLA) was dried in an oven at 60 °C for a minimum of 2.5 h before use to remove any residual water in the polymer. The polymer compositions were prepared through the addition of appropriate amounts of rPLA (60 wt%), castor oil (10 wt%), CB (18 wt%), and graphite (12 wt%) in a chamber of 63 cm^3. All filaments made throughout this work utilised 10 wt% castor oil as a plasticiser.[22] The compounds were mixed using a Thermo Haake Polydrive dynameter fitted with a Thermo Haake Rheomix 600 (Thermo-Haake, Germany) at 190 °C with Banbury rotors at 70 rpm for 5 min. The resulting polymer composites were allowed to cool to room temperature before being granulated to create a finer particle size using a Rapid Granulator 1528 (Rapid, Sweden). The polymer composites were collected and processed through the hopper of a EX2 extrusion line (Filabot, VA, United States). The EX2 was set up with a single screw with a heat zone of 195 °C. The molten polymer was extruded from a 1.75 mm die head, pulled along an Airpath cooling line (Filabot, VA, United States) and collected on a spool. After which, the filament was then ready to use for additive manufacturing.

2.4 Additive manufacturing of the electrodes

All computer designs and 3MF files in this manuscript were produced using Fusion 360® (Autodesk®, CA, United States). These files were sliced and converted to GCODE files in PrusaSlicer (Prusa Research, Prague, Czech Republic). The additive manufactured electrodes were produced using fused filament fabrication (FFF) technology on a Prusa i3 MK3S+ (Prusa Research, Prague, Czech Republic). All additive manufactured electrodes were printed using identical printing

parameters, namely a 0.6 mm nozzle with a nozzle temperature of 215 °C, 100% rectilinear infill,[10] 0.15 mm layer height, and print speed of 35 mm s^{-1}. Electrodes were printed on a smoothed polyetherimide steel sheet heated at 50 °C without the need of application supportive tape or glue.

2.5 Physicochemical characterisation

X-ray photoelectron spectroscopy (XPS) data were acquired using an AXIS Supra (Kratos, UK), equipped with a monochromatic Al X-ray source (1486.6 eV) operating at 225 W and a hemispherical sector analyser. It was operated in fixed transmission mode with a pass energy of 160 eV for survey scans and 20 eV for region scans with the collimator operating in slot mode for an analysis area of approximately 700 × 300 μm, the full-width-at-half-maximum (FWHM) of the Ag 3d5/2 peak using a pass energy of 20 eV was 0.613 eV. The binding energy scale was calibrated by setting the graphitic sp^2 C 1s peak to 284.5 eV; this calibration is acknowledged to be flawed[46] but was nonetheless used in the absence of reasonable alternatives, and because only limited information was to be inferred from absolute peak positions.

Scanning electron microscopy (SEM) micrographs were obtained using a Crossbeam 350 Focussed Ion Beam – Scanning Electron Microscope (FIB-SEM) (Carl Zeiss Ltd., Cambridge, UK) fitted with a field emission electron gun. Secondary electron imaging was completed using a secondary electron secondary ion (SESI) detector. Samples were mounted on the aluminium SEM pin stubs (12 mm diameter, Agar Scientific, Essex, UK) using adhesive carbon tabs (12 mm diameter, Agar Scientific, Essex, UK) and coated with a 5 nm layer of Au/Pd metal using a Leica EM ACE200 coating system before imaging.

Energy dispersive X-ray spectroscopy (EDX) analysis was performed using an Ultim Max 170 detector (Oxford Instruments plc, Abingdon, UK) installed on the FIB-SEM. An acceleration voltage of 20 kV was used to image the samples for EDX analysis experiments. Quantification of the EDX spectra was carried out using a standardless quantification procedure developed by Oxford Instruments and integrated into the AZtec 6.1 software (Oxford Instruments, Abingdon, UK).

X-ray diffraction (XRD) measurements were performed on the powder graphite samples to obtain the structural information using PANalytical X'Pert Powder X-ray diffractometer with Cu (λ = 1.54 Å) as the source with 45 kV voltage and 40 mA current settings. The data were collected in a continuous mode over the 2θ scan range of 5–90°, with a step size of 0.01° for 108 seconds per step at room temperature under ambient conditions. The samples were spinning at 16 rpm during the measurements for uniform data collection. PreFIX module on the incident beam side with the automatic divergence and fixed anti-scatter slit of 4° along with PreFIX module on the diffracted side with PIXcel 1D detector in scanning line mode (1D) with programmable anti-scatter slit were used to collect the diffraction patterns from a constant irradiated length of 0.5 mm.

2.6 Electrochemical experiments

All electrochemical experiments were performed on an Autolab 100N potentiostat controlled by NOVA 2.1.7 (Metrohm, Utrecht, The Netherlands). Identical additively manufactured electrodes were used throughout this work for all filaments, printed in a lollipop shape (Ø 5 mm disc with a connection stem of 8 mm connection length, 2 mm width and 1 mm thickness[11]) alongside an external commercial Ag|AgCl/KCl (3 M) reference electrode with a nichrome wire counter electrode. All solutions of $[Ru(NH_3)_6]^{3+}$ were purged of O_2 thoroughly using N_2 prior to any electrochemical experiments. Solutions of $[Fe(CN)_6]^{4-/3-}$ were prepared in the same way without the need of further degassing. Note that electrochemical cells and additional glassware used in this work has been pre-treated accordingly for trace heavy metals analysis prior to use, which involved a 24 h immersion in 10% nitric acid solution, rinsing with deionised water and keeping in sealed bags to avoid further contamination.

Electrochemical impedance spectroscopy (EIS) was recorded in the frequency range 0.1 Hz to 100 kHz applying 10 mV of signal amplitude to perturb the system under quiescent conditions. NOVA 2.1.7 software was used to fit Nyquist plots obtained to adequate equivalent circuit.

Activation of the additive manufactured electrodes was performed, where applicable, electrochemically in NaOH (0.5 M), as described in the literature.[47] Briefly, the additive manufactured electrodes were connected as the working electrode in conjunction with a nichrome wire coil counter and Ag|AgCl/KCl (3 M) reference electrode and placed in a solution of 0.5 M NaOH. Chronoamperometry was used to activate the additive manufactured electrodes by applying a set voltage of +1.4 V for 200 s, followed by applying −1.0 V for 200 s. The additive manufactured electrodes were then thoroughly rinsed with deionised water and dried under compressed air before further use.

3. Results and discussion

3.1 Green synthesis of gold nanoparticles (AuNPs) on graphite and integration into filament

Sustainability is a key area within the field of additive manufacturing and specifically within additive manufacturing electrochemistry. There is a constant drive for improvement in
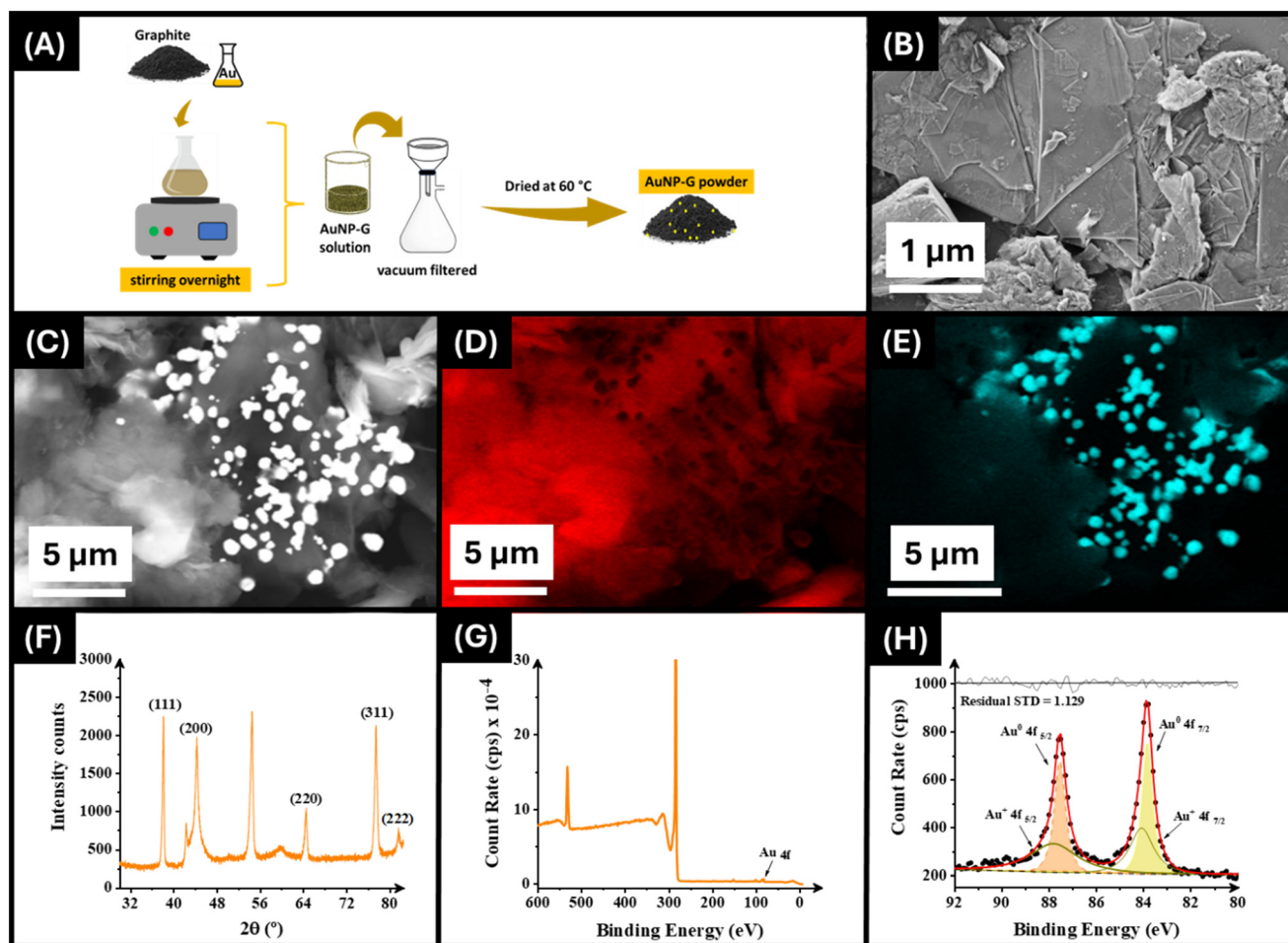

Fig. 1 (A) Schematic representation of AuNP–G production. (B) SEM image for AuNP–G powder. EDX elemental mapping analysis of graphite area (C), carbon map (D), and gold map (E), respectively. (F) XRD pattern of AuNPs. (G) Wide angle XPS and (H) XPS data for AuNPs.

the materials' performance, but this should not come at the detriment to the sustainability of the processes. To further upgrade the performance of previously reported conductive FFF filament, we look to embed AuNPs into the filament to both improve the electrochemical performance and unlock new avenues of research in this field due to the synergy of these precious metal nanoparticles. To achieve this, we look to use graphite as a natural reducing agent for the formation of AuNPs on the surface of the flakes.[45] This synthesis is presented in Fig. 1A, where graphite powder was simply placed within a 20 mg mL^{-1} aqueous solution of gold(III) chloride trihydrate and stirred overnight. Importantly, this synthesis method uses a naturally occurring source of carbon and no additional chemicals as reducing agents, instead relying solely on the natural reducing power of unmodified graphite.

To confirm the presence of the AuNPs on the surface of the graphite flakes initially SEM imaging was performed. Fig. 1B shows a SEM micrograph obtained for this sample where the presence of small spherical-like particles can be seen on the surface of the flakes. To further confirm the presence of gold on the surface of the graphite EDX analysis was undertaken, with the electron image, carbon map, and Au map shown in Fig. 1C–E. Within these maps it can clearly be seen the presence of spherical particles that correspond to Au. Additionally, on spectra analysis the presence of gold at 11 wt%, but only 0.76% atomic weight % was confirmed. Furthermore, X-ray diffraction analysis proved the crystalline nature of gold nanoparticles. The XRD pattern of the synthesised AuNPs on graphite is shown in Fig. 1F. Five distinct Bragg reflections peaks at 38.1°, 44.3°, 64.4°, 77.4° and 81.6° correspond to the lattice planes indexed to the face-centred cubic structure of (111), (200), (220), (311) and (222), respectively (JCPDS No. 04-0784).[48,49]

Finally, XPS analysis was performed on the AuNP–graphite (AuNP–G) filament. The wide-angle scan is presented in Fig. 1G, where there is the presence of a small gold peak. Upon analysis of the Au 4f region, Fig. 1H, we see the clear spectra for two Au peaks corresponding to the Au 4f 7/2 and 5/2, respectively. Adequate fitting of these required each peak to be split into both Au(0) and Au(I) components, producing a fit with an RSD of 1.129, and through atomic analysis, these all appear in approximately equal amounts.

Once the presence of AuNPs was confirmed on the graphite flakes, they were used for the production of electrically conductive additive manufacturing filament. Thermal mixing was chosen due to the environmental benefits over solvent mixing, where there is no need for any additional materials.[18] For this process, graphite and carbon black (CB) were mixed in a 40:60 ratio, previously found to be the optimal composition between these two carbon allotropes.[23,25] In a total carbon loading of 30 wt%, this ratio comprised of 12 wt% AuNP–G, 18 wt% CB, which were added to a thermal mixer set to 190 °C along with 60 wt% recycled PLA (rPLA) and 10 wt% castor oil, a bio-based material which acted as the plasticiser.[22] The presence of castor oil is vital as it contributes to the excellent low-temperature flexibility of the filament, Fig. S1A,† which is important for real commercial use as well as ensuring good printability. These filaments were then used for printing additively manufactured electrodes, Fig. S1B,† which were characterised electrochemically.

3.2 Electrochemical characterisation of the additive manufactured electrodes

After completing the physicochemical characterisation of the bespoke AuNP–graphite (AuNP–G) filament, additively manufactured electrodes were printed, and their electrochemical characterisation performed. This was done through using the near-ideal outer sphere redox probe hexaamineruthenium(III) chloride (1 mM in 0.1 M KCl) and the commonly used inner sphere probe $[Fe(CN)_6]^{4-/3-}$ (1 mM in 0.1 M KCl) to understand the electrochemical performance toward molecules that present different redox mechanisms. Initially, a scan rate study (5–500 mV s^{-1}) was performed as this allowed for the best determination of the heterogeneous electron (charge) transfer rate constant (k^0) and the real electrochemical surface area (A_{real}).[50] Fig. 2 presents an example scan rate study for the AuNP–G electrode where the well-defined peaks correspond to the reduction at ∼−0.25 V and oxidation at ∼−0.1 V for the $[Ru(NH_3)_6]^{3+}$ (1 mM in 0.1 M KCl) redox probe. Inset is the appropriate Randles–Ševčík plot of the peak current *versus* $v^{0.5}$, where the excellent linearity for both oxidation and reduction processes indicates the electrochemical process is of a diffusion-controlled nature.

Using the electrochemical data collected from the scan rate studies within $[Ru(NH_3)_6]^{3+}$ (1 mM in 0.1 M KCl) the key electrochemical parameters of peak-to-peak separation (ΔE_p), k^0, and A_e could be calculated. They are summarised within Table 1 for both the graphite only filament and the AuNP–G filament. It can be seen that the AuNP–G electrode outperforms the unmodified graphite electrode in every parameter. The ΔE_p decreases from 124 (±3) mV to 111 (±5) mV upon the inclusion of AuNPs, the k^0 improves from 1.75 (±0.06) × 10^{-3} cm s^{-1} to 2.04 (±0.08) × 10^{-3} cm s^{-1}, and the A_e increases from 0.53 (±0.04) cm^2 to 0.58 (±0.03) cm^2 upon the incorporation of AuNPs. These improvements are attributed to the high surface area and excellent electrical conductivity provided by AuNPs.

To further test the electrochemical performance of the AuNP–G electrode a scan rate study (5–500 mV s^{-1}) was performed against the inner sphere probe $[Fe(CN)_6]^{4-/3-}$ (1 mM in 0.1 M KCl), Fig. 2C. Once again, clear redox peaks can be seen, which align with the probe, and the excellent linearity shown in the inset with Randles–Ševčík plots confirms the diffusion-controlled nature of the process. Further exploration through electrochemical impedance spectroscopy (EIS) was performed within $[Fe(CN)_6]^{4-/3-}$ (1 mM in 0.1 M KCl) to elucidate the solution resistance (R_S) and charge transfer resistance (R_{CT}) introduced by the AuNP–G electrodes in comparison to the graphite only electrodes. An example of the Nyquist plot obtained is presented in Fig. 2D. Through fitting with the appropriate Randles circuit (inset), the R_S and R_{CT} for each electrode can be elucidated. From Table 1, it can be seen
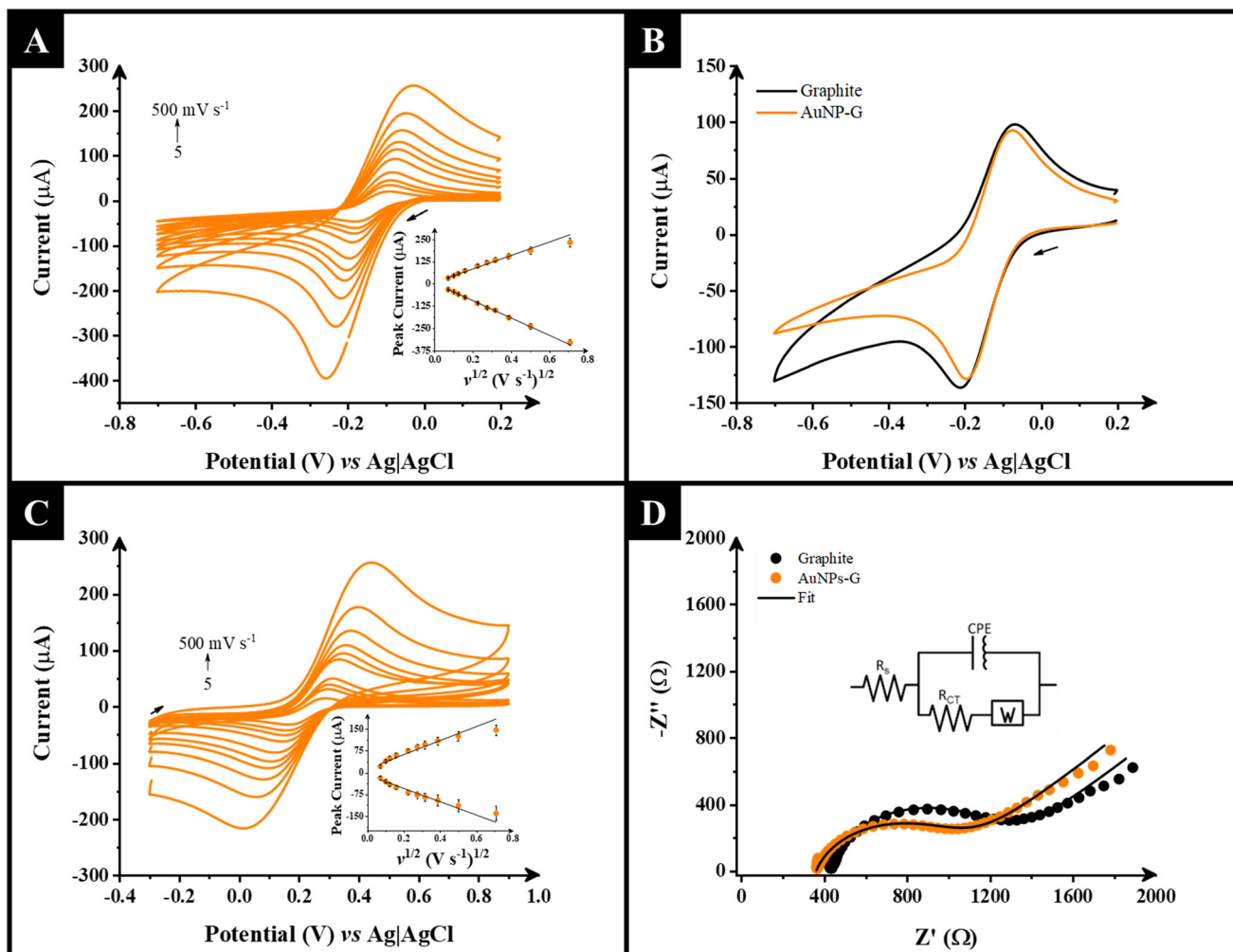
© 2025 The Author(s). Published by the Royal Society of Chemistry

RSC Appl. Interfaces, 2025, **2**, 439–450 | **443**

Fig. 2 (A) Scan rate study (5–500 mV s^{-1}) with $[Ru(NH_3)_6]^{3+}$ (1 mM in 0.1 M KCl) performed using the AuNP–G as the WE. Inset: the Randles–Ševčík plot. (B) CVs (50 mV s^{-1}) with $[Ru(NH_3)_6]^{3+}$ comparing the graphite and AuNP–G electrodes. (C) Scan rate study (5–500 mV s^{-1}) with $[Fe(CN)_6]^{4-/3-}$ (1 mM in 0.1 M KCl) performed using the AuNP–G as the WE. Inset: the Randles–Ševčík plot. (D) EIS Nyquist plots of $[Fe(CN)_6]^{4-/3-}$ comparing graphite and AuNP–G electrodes. Inset: the proposed equivalent circuit.

that the R_S is reduced from 432 ($\pm$ 4) Ω to 362 ($\pm$ 4) Ω when using the AuNP–G electrodes, which is attributed to the conductivity of the AuNPs as it only considers the electrical resistance introduced into the set-up. The R_{CT} also shows an improvement from 806 ($\pm$ 24) Ω to 701 ($\pm$ 14) Ω for the AuNP–G electrode, attributed to both the electrical conductivity of the AuNPs and the increased electrochemical surface area. All of the electrochemical characterisation confirms the presence of

AuNPs on the surface of the graphite flakes improves the electrochemical performance of additively manufactured electrodes printed from these filaments.

3.3 Electroanalytical determination of lead(II)

The detection and quantification of lead (Pb^{2+}) within drinking and surface waters are extremely important analytical

Table 1 Comparison of the electrochemically active area (A_e), heterogeneous electron transfer (k^0), and peak-to-peak separations (ΔE_p) for the bespoke G-only and AuNP–G electrodes

		Additively manufactured electrode	
Probe	Parameter	G-only	AuNP–G
$[Ru(NH_3)_6]^{3+}$	A_{real} (cm^2)	0.53 $\pm$ 0.04	0.58 $\pm$ 0.03
	ΔE_p (V)	0.124 $\pm$ 0.003	0.111 $\pm$ 0.005
	k^0 (cm s^{-1})	1.75 ($\pm$0.06) $\times$ 10^{-3}	2.04 ($\pm$0.08) $\times$ 10^{-3}
$[Fe(CN)_6]^{4-/3-}$	R_S (Ω)	432 $\pm$ 4	362 $\pm$ 4
	R_{CT} (Ω)	806 $\pm$ 24	701 $\pm$ 14

© 2025 The Author(s). Published by the Royal Society of Chemistry

challenges. The toxicity of Pb^{2+} and other heavy metals stems from their ability to bind with protein sites displacing another essential metal. Particularly, lead is known for acting as calcium analogue in the body, thus it is easily absorbed by people with calcium, zinc, and iron deficiencies. Through this mechanism heavy metals can bioaccumulate and cause detrimental effects to the nervous system, kidney, and liver functions, as well as bones and teeth.[51] As such, various regulatory bodies worldwide have placed limits on the concentration of Pb^{2+} within drinking water, with current EU limits aiming to be reduced from 10 μg L^{-1} (10 ppb) to 5 μg L^{-1} (5 ppb) by 2036.[52] This is therefore the threshold that electroanalytical sensors in this field are required to reach.

In this work, the detection of Pb^{2+} was first explored using both square wave anodic stripping voltammetry (SWASV) and differential pulse anodic stripping voltammetry (DPASV), with Britton Robinson buffer (pH = 5.0) and HCl (0.1 M) as the electrolytes. Fig. 3A shows the results in HCl. It can be seen

that SWASV gave a better response, with a clear and sharp voltametric peak obtained at the appropriate stripping potential for Pb^{2+} and that HCl was a suitable electrolyte for this application, in agreement with the literature.[53] As such, SWASV and 0.1 M HCl were chosen to complete further work. Using SWV, the deposition potential and deposition times were next optimised, Fig. S2 and S3,† for both 10 and 100 ppb Pb^{2+} concentration levels, with −1.1 V and 120 s being the best conditions optimised for the detection of lower concentrations of Pb^{2+} and −0.9 V and 90 s for higher concentration of Pb^{2+}, respectively. Further optimisation of the SWASV methodology was performed, as summarised in Table S1,† where the step potential, amplitude and frequencies were optimised at 0.009 V, 0.06 V and 40 Hz respectively. Note that the optimisation of these instrumental parameters was not affected by testing different concentrations of Pb^{2+}. Finally, according to the described activation procedures in acidic media involving the detection
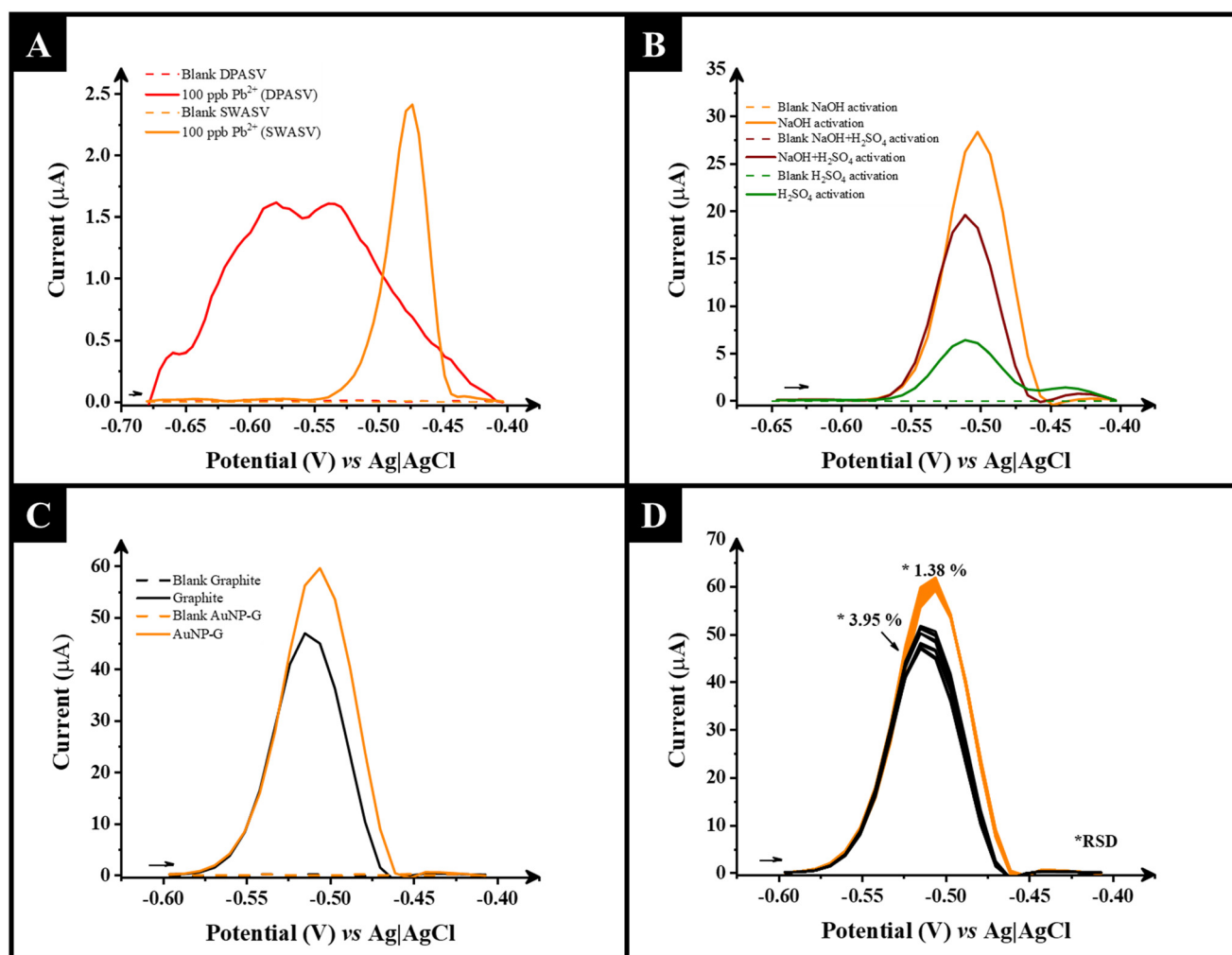

Fig. 3 (A) Comparison between SWASV and DPASV performed at AuNP–G electrode with 100 ppb of Pb^{2+} and quiescent conditions during deposition steps. (B) SWASV results for different activation methods. (C) SWASV in the presence of 100 ppb of Pb^{2+} performed at graphite and AuNP–G electrodes and (D) repetitive measurements ($n = 10$) using the graphite and AuNP–G electrodes. SWASV parameters: $a = 60$ mV, $f = 40$ Hz, $\Delta E = 9$ mV, $E_{deposition} = -0.9$ V, and $t_{deposition} = 90$s. DPASV parameters: $a = 25$ mV, $t = 0.025$ s, $\Delta E = 5$ mV, $E_{deposition} = -0.70$ V, and $t_{deposition} = 60$s.

© 2025 The Author(s). Published by the Royal Society of Chemistry

RSC Appl. Interfaces, 2025, 2, 439–450 | 445

the G-electrode could only detect a minimum concentration of 3 ppb. Likewise, higher sensitivity values were achieved for AuNP–G (37 nA ppb^{-1}) compared to only G-electrode (140 nA ppb^{-1}). The limit of detection (LoD) and limit of quantification (LoQ) were determined using 3 and 10 times the standard deviation of the blank divided by the value of the slopes. For the AuNP–G electrodes these were calculated at 0.89 ppb and 2.97 ppb respectively. This showed that the AuNP–G electrodes are suitable for use against the current standards (5–10 ppb) and offered significant improvement on the G-only electrodes which produced values of 2.57 ppb and 8.57 ppb. Further comparison of the performance of the AuNP–G electrodes against literature reports can be seen in Table S2,† where these electrodes compare excellently.

Possible interferents were then tested regarding both the G-only, Fig. 4C, and AuNP–G, Fig. 4D, electrodes. The anodic current responses of the electrodes were tested in the presence of 1:5 analyte to interferent ratio for Cd^{2+}, Hg^{2+} and As^{3+}. When using G-only electrodes, there was a noticeable decrease in the peak current for Pb when Cd and Hg were present and a substantial increase (164%) in the Pb peak current in the presence of As. However, the AuNP–G electrode demonstrated greater resistance to interference from other species. The presence of Hg^{2+} and As^{3+} did not cause significant interference, while Cd led to a positive effect, increasing the Pb peak current by 35%. In all cases there was a significant improvement in the performance when using the AuNP–G electrodes.

3.4 Electroanalytical application for lead(ɪɪ) in environmental water

To demonstrate the applicability of the methodology developed using G-only and AuNP–G additive manufactured electrodes, real sample analysis towards Pb^{2+} detection in river water was carried out. Fig. 5A and B show the voltammetric responses, with the linear plots corresponding to standard addition calibrations, for both the G-only and AuNP–G electrodes, respectively. Using these plots, recovery values were calculated at 137% for the G-only and 106% for the AuNP–G electrodes, showing once again that the AuNPs within the filament improve the overall electroanalytical performance of the electrodes towards Pb^{2+} detection.

This work presents a simple and eco-friendly way to incorporate metallic gold nanoparticles into additive manufacturing filament while maintaining the integrity of PLA polymer matrix. This filament offers significant improvements in terms of both conductivity, electrochemical and electroanalytical performance despite the low metal loading provided. The incorporation of this vital nanomaterial into additive manufacturing filament for the first time offers a paradigm shift in additive manufacturing electrochemistry where only carbon conductive polymers developed to date present important limitations. This opens the field to a plethora of new areas where AuNPs play a crucial role, such as biosensing applications. Importantly, this work achieves this without the need for post-print modification of electrodes, using standard additive manufacturing instrumentation, as well as utilising a sustainable nanoparticle synthesis approach.

4. Conclusions

In this work, we report the inclusion of AuNPs within additive manufacturing filament through an eco-friendly synthesis methodology. The AuNPs were formed on the surface of graphite overnight, where the graphite flakes act as a natural reducing agent. The presence of AuNPs on the surface of the graphite flakes was confirmed through XRD, XPS, SEM and EDX analysis. The AuNP-modified graphite was then incorporated into conductive additive manufacturing filament
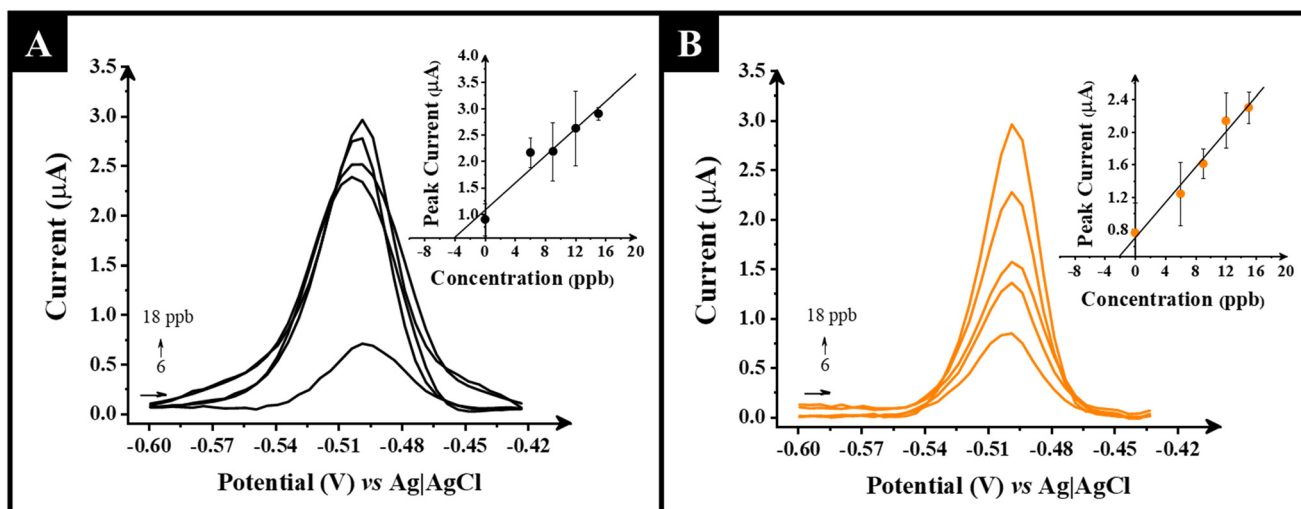

Fig. 5 SWASV for Pb^{2+} in diluted river water (50-fold) in HCl 0.1 M performed at (A) graphite and (B) AuNP–G electrodes in a concentration range of 6 to 18 ppb (6, 9, 12, 15, and 18 ppb). SWASV parameters: a = 60 mV, f = 40 Hz, ΔE = 9 mV, $E_{deposition}$ = −1.1 V, and $t_{deposition}$ = 120 s. Insets: calibration curves obtained by the standard addition method.

© 2025 The Author(s). Published by the Royal Society of Chemistry

RSC Appl. Interfaces, 2025, **2**, 439–450 | **447**

in an optimum ratio with carbon black. These electrodes produced an enhanced electrochemical performance in hexaammineruthenium(III) chloride with the ΔE_p decreasing from 124 (±3) mV to 111 (±5) mV upon the inclusion of AuNPs, the k^0 improving from 1.75 (±0.06) × 10^{-3} cm s^{-1} to 2.04 (±0.08) × 10^{-3} cm s^{-1}, and the A_e increasing from 0.53 (±0.04) cm^2 to 0.58 (±0.03) cm^2 upon the inclusion of AuNPs. The electrochemical performance was also seen to significantly improve toward inner-sphere redox probes. Finally, the electroanalytical performance was tested toward the detection of Pb^{2+}, whereby a linear range between 1–75 ppb, with a sensitivity of 37 nA ppb^{-1} and an R^2 value of 0.98 was achieved alongside an LoD and LoQ of 0.89 ppb and 2.97 ppb respectively. This work presents a paradigm shift in the development of conductive additive manufacturing filament, whereby metallic gold nanoparticles can be embedded within the filament, removing the need for post-print modification. We expect this work to open up a plethora of research avenues due to the synergy between AuNPs and various electrochemical platforms.

Data availability

Data is available from the corresponding author.

Conflicts of interest

There are no conflicts of interest to declare.

Acknowledgements

References

1 M. Attaran, The rise of 3-D printing: The advantages of additive manufacturing over traditional manufacturing, *Bus. Horiz.*, 2017, **60**, 677–688.

2 Y. Y. C. Choong, H. W. Tan, D. C. Patel, W. T. N. Choong, C.-H. Chen and H. Y. Low, et al., The global rise of 3D printing during the COVID-19 pandemic, *Nat. Rev. Mater.*, 2020, **5**, 637–639.

3 M. J. Whittingham, R. D. Crapnell and C. E. Banks, Additively manufactured rotating disk electrodes and experimental setup, *Anal. Chem.*, 2022, **94**, 13540–13548.

4 M. J. Whittingham, R. D. Crapnell, E. J. Rothwell, N. J. Hurst and C. E. Banks, Additive manufacturing for electrochemical labs: An overview and tutorial note on the production of cells, electrodes and accessories, *Talanta*, 2021, **4**, 100051.

5 A. G.-M. Ferrari, N. J. Hurst, E. Bernalte, R. D. Crapnell, M. J. Whittingham and D. A. Brownson, et al., Exploration of defined 2-dimensional working electrode shapes through additive manufacturing, *Analyst*, 2022, **147**, 5121–5129.

6 R. D. Crapnell, E. Bernalte, A. G.-M. Ferrari, M. J. Whittingham, R. J. Williams and N. J. Hurst, et al., All-in-one single-print additively manufactured electroanalytical sensing platforms, *ACS Meas. Sci. Au*, 2021, **2**, 167–176.

7 A. Abdalla and B. A. Patel, 3D printed electrochemical sensors, *Annu. Rev. Anal. Chem.*, 2021, **14**, 47–63.

8 R. M. Cardoso, C. Kalinke, R. G. Rocha, P. L. Dos Santos, D. P. Rocha and P. R. Oliveira, et al., Additive-manufactured (3D-printed) electrochemical sensors: A critical review, *Anal. Chim. Acta*, 2020, **1118**, 73–91.

9 J. Muñoz and M. Pumera, Accounts in 3D-printed electrochemical sensors: towards monitoring of environmental pollutants, *ChemElectroChem*, 2020, **7**, 3404–3413.

10 E. Bernalte, R. D. Crapnell, O. M. Messai and C. E. Banks, The Effect of Slicer Infill Pattern on the Electrochemical Performance of Additively Manufactured Electrodes, *ChemElectroChem*, 2024, **11**, e202300576.

11 R. D. Crapnell, A. Garcia-Miranda Ferrari, M. J. Whittingham, E. Sigley, N. J. Hurst and E. M. Keefe, et al., Adjusting the connection length of additively manufactured electrodes changes the electrochemical and electroanalytical performance, *Sensors*, 2022, **22**, 9521.

12 R. Shergill and B. Patel, The effects of material extrusion printing speed on the conductivity of carbon black/polylactic acid electrodes, *ChemElectroChem*, 2022, **9**, e202200831.

13 R. S. Shergill, C. L. Miller and B. A. Patel, Influence of instrument parameters on the electrochemical activity of 3D printed carbon thermoplastic electrodes, *Sci. Rep.*, 2023, **13**, 339.

14 C. Kalinke, N. V. Neumsteir, G. de Oliveira Aparecido, T. V. de Barros Ferraz, P. L. Dos Santos and B. C. Janegitz, et al., Comparison of activation processes for 3D printed PLA-graphene electrodes: electrochemical properties and application for sensing of dopamine, *Analyst*, 2020, **145**, 1207–1218.

15 D. P. Rocha, R. G. Rocha, S. V. Castro, M. A. Trindade, R. A. Munoz and E. M. Richter, et al., Posttreatment of 3D-printed surfaces for electrochemical applications: A critical review on proposed protocols, *Electrochem. Sci. Adv.*, 2022, **2**, e2100136.

16 R. S. Shergill and B. A. Patel, Preprinting saponification of carbon thermoplastic filaments provides ready-to-use electrochemical sensors, *ACS Appl. Electron. Mater.*, 2023, **5**, 5120–5128.

17 R. S. Shergill, F. Perez, A. Abdalla and B. A. Patel, Comparing electrochemical pre-treated 3D printed native and mechanically polished electrode surfaces for analytical sensing, *J. Electroanal. Chem.*, 2022, **905**, 115994.

18 R. D. Crapnell, C. Kalinke, L. R. G. Silva, J. S. Stefano, R. J. Williams and R. A. A. Munoz, et al., Additive manufacturing

electrochemistry: an overview of producing bespoke conductive additive manufacturing filaments, *Mater. Today*, 2023, **71**, 73–90.

19 P. Wuamprakhon, R. D. Crapnell, E. Sigley, N. J. Hurst, R. J. Williams and M. Sawangphruk, *et al.*, Recycled Additive Manufacturing Feedstocks for Fabricating High Voltage, Low-Cost Aqueous Supercapacitors, *Adv. Sustainable Syst.*, 2023, **7**, 2200407.

20 E. Sigley, C. Kalinke, R. D. Crapnell, M. J. Whittingham, R. J. Williams and E. M. Keefe, *et al.*, Circular economy electrochemistry: creating additive manufacturing feedstocks for caffeine detection from post-industrial coffee pod waste, *ACS Sustainable Chem. Eng.*, 2023, **11**, 2978–2988.

21 I. V. Arantes, R. D. Crapnell, M. J. Whittingham, E. Sigley, T. R. Paixão and C. E. Banks, Additive manufacturing of a portable electrochemical sensor with a recycled conductive filament for the detection of atropine in spiked drink samples, *ACS Appl. Eng. Mater.*, 2023, **1**, 2397–2406.

22 R. D. Crapnell, I. V. Arantes, M. J. Whittingham, E. Sigley, C. Kalinke and B. C. Janegitz, *et al.*, Utilising bio-based plasticiser castor oil and recycled PLA for the production of conductive additive manufacturing feedstock and detection of bisphenol A, *Green Chem.*, 2023, **25**, 5591–5600.

23 I. V. Arantes, R. D. Crapnell, E. Bernalte, M. J. Whittingham, T. R. Paixão and C. E. Banks, Mixed graphite/carbon black recycled PLA conductive additive manufacturing filament for the electrochemical detection of oxalate, *Anal. Chem.*, 2023, **95**, 15086–15093.

24 R. D. Crapnell, I. V. Arantes, J. R. Camargo, E. Bernalte, M. J. Whittingham and B. C. Janegitz, *et al.*, Multi-walled carbon nanotubes/carbon black/rPLA for high-performance conductive additive manufacturing filament and the simultaneous detection of acetaminophen and phenylephrine, *Microchim. Acta*, 2024, **191**, 96.

25 K. K. Augusto, R. D. Crapnell, E. Bernalte, S. Zighed, A. Ehamparanathan and J. L. Pimlott, *et al.*, Optimised graphite/carbon black loading of recycled PLA for the production of low-cost conductive filament and its application to the detection of β-estradiol in environmental samples, *Microchim. Acta*, 2024, **191**, 375.

26 E. Koukouviti, A. Economou and C. Kokkinos, 3D Printable Multifunctional Electrochemical Nano-Doped Biofilament, *Adv. Funct. Mater.*, 2024, 2402094.

27 S. Guo and E. Wang, Synthesis and electrochemical applications of gold nanoparticles, *Anal. Chim. Acta*, 2007, **598**, 181–192.

28 G. Siciliano, A. Alsadig, M. S. Chiriacò, A. Turco, A. Foscarini and F. Ferrara, *et al.*, Beyond traditional biosensors: Recent advances in gold nanoparticles modified electrodes for biosensing applications, *Talanta*, 2024, **268**, 125280.

29 T. Xiao, J. Huang, D. Wang, T. Meng and X. Yang, Au and Au-Based nanomaterials: Synthesis and recent progress in electrochemical sensor applications, *Talanta*, 2020, **206**, 120210.

30 A. G.-M. Ferrari, P. Carrington, S. J. Rowley-Neale and C. E. Banks, Recent advances in portable heavy metal

electrochemical sensing platforms, *Environ. Sci.: Water Res. Technol.*, 2020, **6**, 2676–2690.

31 S. Alim, J. Vejayan, M. M. Yusoff and A. Kafi, Recent uses of carbon nanotubes & gold nanoparticles in electrochemistry with application in biosensing: A review, *Biosens. Bioelectron.*, 2018, **121**, 125–136.

32 C. Y. Foo, H. N. Lim, M. A. Mahdi, M. H. Wahid and N. M. Huang, Three-dimensional printed electrode and its novel applications in electronic devices, *Sci. Rep.*, 2018, **8**, 7399.

33 A. M. L. Marzo, C. C. Mayorga-Martinez and M. Pumera, 3D-printed graphene direct electron transfer enzyme biosensors, *Biosens. Bioelectron.*, 2020, **151**, 111980.

34 E. H. Z. Ho, A. Ambrosi and M. Pumera, Additive manufacturing of electrochemical interfaces: simultaneous detection of biomarkers, *Appl. Mater. Today*, 2018, **12**, 43–50.

35 J. Turkevich, P. C. Stevenson and J. Hillier, A study of the nucleation and growth processes in the synthesis of colloidal gold, *Discuss. Faraday Soc.*, 1951, **11**, 55–75.

36 B. Enustun and J. Turkevich, Coagulation of colloidal gold, *J. Am. Chem. Soc.*, 1963, **85**, 3317–3328.

37 P. Laaksonen, J. Kivioja, A. Paananen, M. Kainlauri, K. Kontturi and J. Ahopelto, *et al.*, Selective nanopatterning using citrate-stabilized Au nanoparticles and cystein-modified amphiphilic protein, *Langmuir*, 2009, **25**, 5185–5192.

38 J. Hu, F. Li, K. Wang, D. Han, Q. Zhang and J. Yuan, *et al.*, One-step synthesis of graphene–AuNPs by HMTA and the electrocatalytic application for O_2 and H_2O_2, *Talanta*, 2012, **93**, 345–349.

39 V. Duc Chinh, G. Speranza, C. Migliaresi, N. Van Chuc, V. Minh Tan and N.-T. Phuong, Synthesis of gold nanoparticles decorated with multiwalled carbon nanotubes (Au-MWCNTs) via cysteaminium chloride functionalization, *Sci. Rep.*, 2019, **9**, 5667.

40 D. Grumelli, C. Vericat, G. Benitez, M. Vela, R. Salvarezza and L. Giovanetti, *et al.*, Thiol-capped gold nanoparticles on graphite: Spontaneous adsorption and electrochemically induced release, *J. Phys. Chem. C*, 2007, **111**, 7179–7184.

41 J. R. Camargo, R. D. Crapnell, E. Bernalte, A. J. Cunliffe, J. Redfern and B. C. Janegitz, *et al.*, Conductive recycled PETg additive manufacturing filament for sterilisable electroanalytical healthcare sensors, *Appl. Mater. Today*, 2024, **39**, 102285.

42 R. D. Crapnell, E. Bernalte, E. Sigley and C. E. Banks, Recycled PETg embedded with graphene, multi-walled carbon nanotubes and carbon black for high-performance conductive additive manufacturing feedstock, *RSC Adv.*, 2024, **14**, 8108–8115.

43 T. R. Walker, (Micro) plastics and the UN sustainable development goals, *Curr. Opin. Green Sustainable Chem.*, 2021, **30**, 100497.

44 N. German, A. Ramanavicius and A. Ramanaviciene, Electrochemical deposition of gold nanoparticles on graphite rod for glucose biosensing, *Sens. Actuators, B*, 2014, **203**, 25–34.

45 R. K. Pandey, L. Chen, S. Teraji, H. Nakanishi and S. Soh, Eco-friendly, direct deposition of metal nanoparticles on

© 2025 The Author(s). Published by the Royal Society of Chemistry

RSC Appl. Interfaces, 2025, **2**, 439–450 | **449**

graphite for electrochemical energy conversion and storage, *ACS Appl. Mater. Interfaces*, 2019, **11**, 36525–36534.

46 G. Greczynski and L. Hultman, The same chemical state of carbon gives rise to two peaks in X-ray photoelectron spectroscopy, *Sci. Rep.*, 2021, **11**, 1–5.

47 E. M. Richter, D. P. Rocha, R. M. Cardoso, E. M. Keefe, C. W. Foster and R. A. Munoz, *et al.*, Complete additively manufactured (3D-printed) electrochemical sensing platform, *Anal. Chem.*, 2019, **91**, 12844–12851.

48 S. Krishnamurthy, A. Esterle, N. C. Sharma and S. V. Sahi, Yucca-derived synthesis of gold nanomaterial and their catalytic potential, *Nanoscale Res. Lett.*, 2014, **9**, 627.

49 D. Philip, Rapid green synthesis of spherical gold nanoparticles using Mangifera indica leaf, *Spectrochim. Acta, Part A*, 2010, **77**, 807–810.

50 R. D. Crapnell and C. E. Banks, Perspective: What constitutes a quality paper in electroanalysis?, *Talanta*, 2021, **4**, 100065.

51 M. S. Collin, S. K. Venkatraman, N. Vijayakumar, V. Kanimozhi, S. M. Arbaaz and R. G. S. Stacey, *et al.*, Bioaccumulation of lead (Pb) and its effects on human: A review, *J. Hazard. Mater. Adv.*, 2022, **7**, 100094.

52 *Directive (EU) 2020/2184 of the European Parliament and of the Council of 16 December 2020 on the quality of water intended for human consumption*, Official Journal of the European Union, 2020.

53 E. Bernalte, S. Arévalo, J. Pérez-Taborda, J. Wenk, P. Estrela and A. Avila, *et al.*, Rapid and on-site simultaneous electrochemical detection of copper, lead and mercury in the Amazon river, *Sens. Actuators, B*, 2020, **307**, 127620.

54 E. Bernalte, C. M. Sánchez and E. P. Gil, Determination of mercury in ambient water samples by anodic stripping voltammetry on screen-printed gold electrodes, *Anal. Chim. Acta*, 2011, **689**, 60–64.